Excitation-emission Fourier-transform spectroscopy based on a birefringent interferometer

ANTONIO PERRI,[1,#] FABRIZIO PREDA,[1,#] COSIMO D'ANDREA,[1,2] ERLING THYRHAUG,[3] GIULIO CERULLO,[1] DARIO POLLI,[1,2*] AND JÜRGEN HAUER[3]

[1]IFN-CNR and Dipartimento di Fisica, Politecnico di Milano, Piazza L. da Vinci 32, 20133 Milano, Italy
[2]Center for Nano Science and Technology at Polimi, Istituto Italiano di Tecnologia, 20133Milano, Italy
[3]Photonics Institute, TU Wien, Gusshausstrasse 27, 1040 Vienna, Austria
 # these authors contributed equally
**dario.polli@polimi.it*

Abstract: The correlation of molecular excitation and emission events provides a powerful multidimensional spectroscopy tool, by relating transitions from electronic ground and excited states through two-dimensional excitation-emission maps. Here we present a compact, fast and versatile Fourier-transform spectrometer, combining absorption and excitation-emission fluorescence spectroscopy in the visible. We generate phase-locked excitation pulse pairs via an inherently stable birefringent wedge-based common-path interferometer, retaining all the advantages of Fourier-transform spectroscopy but avoiding active stabilization or auxiliary tracking beams. We employ both coherent and incoherent excitation sources on dye molecules in solution, with data acquisition times in the range of seconds and minutes, respectively.

© 2017 Optical Society of America. One print or electronic copy may be made for personal use only. Systematic reproduction and distribution, duplication of any material in this paper for a fee or for commercial purposes, or modifications of the content of this paper are prohibited. Link to the online abstract in the OSA Journal: https://doi.org/10.1364/OE.25.00A483

OCIS codes: (300.6300) Spectroscopy, Fourier transforms; (120.3180) Interferometry; (300.2530) Fluorescence, laser-induced.

References and links

1. J. R. Lakowicz, *Principles of Fluorescence Spectroscopy* (Springer Science & Business Media, New York, USA, 2007).
2. N. J. Reilly, T. W. Schmidt, and S. H. Kable, "Two-dimensional fluorescence (excitation/emission) spectroscopy as a probe of complex chemical environments," J. Phys. Chem. A **110**(45)**,** 12355–12359 (2006).
3. J. R. Gascooke, U. N. Alexander, and W. D. Lawrance, "Two dimensional laser induced fluorescence spectroscopy: A powerful technique for elucidating rovibronic structure in electronic transitions of polyatomic molecules," J. Chem. Phys. **134**(18), 184301 (2011).
4. Á. Andrade-Eiroa, M. Canle, and V. Cerdá, "Environmental Applications of Excitation-Emission Spectrofluorimetry: An In-Depth Review II", Appl. Spectrosc. Rev. **48**, 77–141 (2013).
5. P.G Coble, "Characterization of marine and terrestrial DOM in seawater using excitation-emission matrix spectroscopy", Marine Chemistry **51**, 325–346 (1996).
6. R. S. DaCosta, H. Andersson, and B. C. Wilson, "Molecular Fluorescence Excitation–Emission Matrices Relevant to Tissue Spectroscopy", Photochem. Photobiol. **78**, 384–392 (2003).
7. S. J. Leavesley, M. Walters, C. Lopez, T. Baker, P. F. Favreau, T. C. Rich, P. F. Rider, and C. W. Boudreaux, "Hyperspectral imaging fluorescence excitation scanning for colon cancer detection", J. Biomed. Opt. **21**, 104003 (2016).
8. N. Ramanujam, "Fluorescence Spectroscopy of Neoplastic and Non-Neoplastic Tissues", Neoplasia **2**, 89–117 (2000).
9. J. Christensen, L. Nørgaard, R. Bro, and S. B. Engelsen, "Multivariate Autofluorescence of Intact Food Systems" Chem. Rev. **106**, 1979–1994 (2006).
10. B. DeCoster, R. L. Christensen, R. Gebhard, J. Lugtenburg, R. Farhoosh, and H. A. Frank, "Low-lying electronic states of carotenoids," BBA - Bioenergetics **1102**(1), 107–114 (1992).
11. J. G. Hirschberg, G. Vereb, C. K. Meyer, A. K. Kirsch, E. Kohen, and T. M. Jovin, "Interferometric measurement of fluorescence excitation spectra," Appl. Opt. **37**(10), 1953–1957 (1998).
12. H Anzai, N. K. Joshi, M. Fuyuki, and A. Wada, "Fourier transform two-dimensional fluorescence excitation spectrometer by using tandem Fabry-Perot interferometer," Rev. Sci. Instrum. **86**(1), 014101 (2015).

13. L. Piatkowski, E. Gellings, and N. F. van Hulst, "Broadband single-molecule excitation spectroscopy," Nature Comm. **7**, 10411 (2016).
14. R. J. Bell, *Introductory Fourier Transform Spectroscopy* (Academic, 1972).
15. S. P. Davis, M. C. Abrams, and J. W. Brault, *Fourier Transform Spectrometry* (Academic, 2001).
16. D. Brida, C. Manzoni, and G. Cerullo, "Phase-locked pulses for two-dimensional spectroscopy by a birefringent delay line," Opt. Lett. **37**(15), 3027–3029 (2012).
17. J. Réhault, M. Maiuri, A. Oriana, and G. Cerullo, "Two-dimensional electronic spectroscopy with birefringent wedges," Rev. Sci. Instrum. **85**(12), 123107 (2014).
18. J. Réhault, M. Maiuri, C. Manzoni, D. Brida, J. Helbing, and G. Cerullo, "2D IR spectroscopy with phase-locked pulse pairs from a birefringent delay line," Opt. Express **22**(8), 9063–9072 (2014).
19. R. Borrego-Varillas, A. Oriana, L. Ganzer, A. Trifonov, I. Buchvarov, C. Manzoni, and G. Cerullo, "Two-dimensional electronic spectroscopy in the ultraviolet by a birefringent delay line," Opt. Express **24**(25), 28491–28499 (2016).
20. A. Oriana, J. Réhault, F. Preda, D. Polli, and G. Cerullo, "Scanning Fourier transform spectrometer in the visible range based on birefringent wedges," J. Opt. Soc. Am. A **33**(7), 1415–1420 (2016).
21. F. Preda, A. Oriana, J. Réhault, L. Lombardi, A. C. Ferrari, G. Cerullo and D. Polli, "Linear and nonlinear spectroscopy by a common-path birefringent interferometer", IEEE J. Sel. Topics Quantum Electron. **23**, 1–9 (2017)
22. P. Jacquinot, "New Developments in Interference Spectroscopy," Rep. Progr. Phys. **23**, 268–312 (1960).
23. J. M. Dixon, M. Taniguchi, and J. S. Lindsey, "PhotochemCAD 2: A Refined Program with Accompanying Spectral Databases for Photochemical Calculations," Photochem. Photobiol. **81**(1), 212–213 (2005).
24. J. Réhault, F. Crisafi, V. Kumar, G. Ciardi, M. Marangoni, G. Cerullo, and D. Polli, "Broadband stimulated Raman scattering with Fourier-transform detection," Opt. Expr. **23**(19), 25235–25246 (2015).
25. L. Peng, J. T. Motz, R. W. Redmond, B. E. Bouma, and G. J. Tearney, "Fourier transform emission lifetime spectrometer," Opt. Lett. **32**, 421–423 (2007).

1. Introduction

Optical spectroscopy is an essential tool for the study of light-matter interactions and for the investigation of molecular processes, with time resolution unrivalled by any other technique. The simplest forms of optical spectroscopy are the measurement of absorption and emission spectra, which provide important chemico-physical information about the sample under study. Specifically, fluorescence spectroscopy is intensively used for the study of biological specimens, from the molecular to the tissue level, both *in vitro* and *in vivo* [1]. Absorption and fluorescence spectra are linear in light intensity and one-dimensional in the sense that the only changeable parameter is the excitation or emission frequency. Excitation-emission matrix (EEM) spectroscopy is a powerful extension of fluorescence spectroscopy, which records emission spectra as a function of excitation frequency, building a two-dimensional (2D) map. EEM spectroscopy provides a rich database for the analysis of congested electronic transitions in the gas [2-3] and condensed phase [4-9] for the study of different materials, from inorganic samples to environmental applications [4-5], from biological specimens [6-8] to food analysis [9]. The simultaneous measurement of EEM maps and absorption spectra is beneficial for the study of energy transfer processes, as deviations between the two signals are indicative of loss channels [10].

EEM maps are typically measured in the frequency domain, by selecting a narrowband frequency slice of a broadband excitation light, recording the corresponding fluorescence spectra and finally stacking the data. This generally leads to long acquisition times, due to the need to scan the excitation and/or emission wavelength, and to a bulky setup including two monochromators [1]. The use of the latter can be avoided by employing broadband spectral interferometric techniques to record the signal [11-13]. Here, an interferometer generates two delayed replicas of the excitation light, and the fluorescence signal is detected as a function of their time-delay t_1. Excitation-frequency-resolved signals are then obtained via Fourier-transformation (FT) from the time domain [14-15]. Since the fluorescence signal as a function of t_1 oscillates with the period of the carrier wave, the FT operation requires interferometric stability of the excitation wave pair, i.e. control of their optical path difference to within a small fraction of their carrier wavelength, which is challenging to achieve in the visible range. Recently, we introduced a birefringent common-path interferometer for FT-spectroscopy,

called the Translating-Wedge-based Identical pulses eNcoding System (TWINS) [16]. Briefly, TWINS introduces the required delay t_1 via birefringence: two orthogonal polarization components experience different delays when passing through a birefringent wedge pair of variable material thickness. For the purposes of time-resolved spectroscopy, TWINS has already been implemented successfully in the visible [17], IR [18] and UV [19] spectral ranges. TWINS was also employed for the measurement of steady state absorption spectra, as part of a time-domain scanning FT absorption spectrometer [20-21].

In this paper, we show that TWINS is readily adapted to be used as a combined EEM- and absorption spectrometer, where both measurements are recorded simultaneously and with visible light. This spectrometer yields steady-state EEM maps, with adjustable excitation wavelength resolution (down to the sub-nm range) set by the TWINS scan range, and frequency dispersed detection using a standard CCD detector. The TWINS-based spectrofluorometer presented here employs only conventional optical components and fully retains all advantages of FT spectrometers, namely: high throughput and an increase of the system étendue due to the lack of optical slits (Jacquinot's advantage [22]); high excitation frequency accuracy based on reliable calibration procedures (Connes' advantage); broad wavelength coverage in the emission, as defined by standard CCD detectors. We compare the performance of a cost effective LED lamp and a supercontinuum laser as excitation sources. Our TWINS-based spectrofluorometer presents two main advantages over the conventional frequency-domain devices: (1) faster acquisition times, due to parallel illumination of the sample with a broad excitation light, thus increasing the fluorescence emission; (2) compactness (especially in the case of illumination with a LED), a key aspect to foster the use of the system outside a laboratory environment, e.g. in bio-medical and environmental applications.

2. Experimental setup

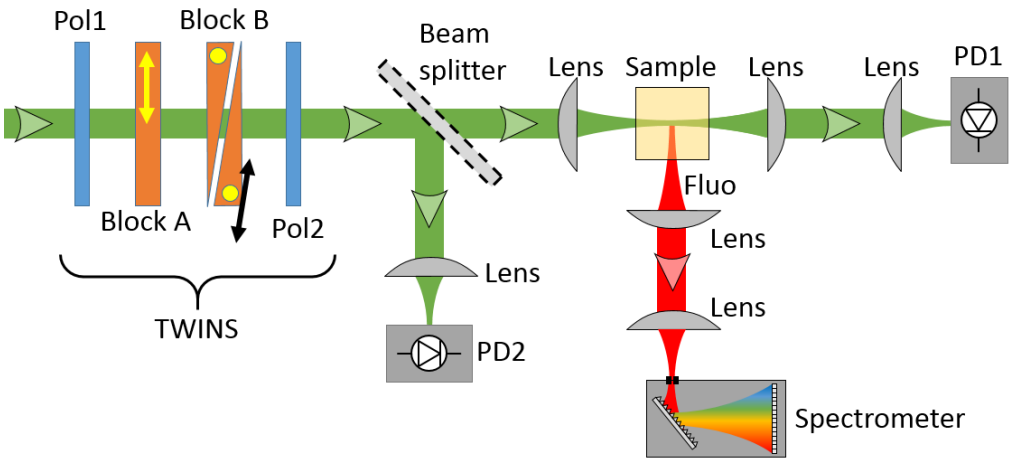

Fig. 1. Experimental setup used for combined EEM and absorption measurements. Pol1, Pol2: polarizers; PD1, PD2: photodiodes. Black arrow indicates the direction of movement of the translating wedge. The yellow arrow and dots indicate the orientations of the optical axes of the birefringent optical elements.

Figure 1 shows the experimental setup of the combined EEM/absorption spectrometer. We performed photoexcitation with both a coherent and an incoherent light source. For coherent excitation, we used a high-power supercontinuum fiber laser (NKT Photonics model SuperK Extreme EXW-12), emitting an ultra-broadband spectrum in the 500–2300 nm range (see Fig. 2(a)) with a power density higher than 2 mW/nm in the 550-1000 nm spectral region. As an incoherent light source, we employed a commercial white-light battery-supplied LED lamp (Varta, Germany), emitting 150 lumens over the 400-700 nm wavelength range. The excitation light is sent to a common-path interferometer, which is a simplified version of the TWINS

interferometer introduced in ref. [16] for 2D electronic spectroscopy. Briefly, the setup consists of two birefringent blocks, A and B, with optical axes rotated by 90° with respect to each other and perpendicular to the propagation direction of the beam. For an input beam polarization, set by polarizer Pol1, at 45° with respect to the optical axes, block A introduces a fixed delay between the two orthogonally polarized components that propagate along the fast and slow axes of the material. Block B introduces a delay of opposite sign with respect to block A, thus allowing a change of delay from positive to negative values. To enable fine tuning of the delay, block B is shaped in the form of two wedges with the same apex angle, one of which is mounted on a computer-controlled precision translation stage (LMS-60 Linear Motor Stage, Physik Instrumente). Finally, polarizer Pol2 projects the two delayed replicas to a common polarization state, allowing their interference on the detector.

For the experiments reported here, we used wedges of lithium niobate ($LiNbO_3$, manufactured by Foctek Photonics Inc., Fuzhou, China) with α=10° apex angle and 45-mm lateral size. Considering the average birefringence of $LiNbO_3$ $\Delta n=n_o-n_e=0.1$, where n_o(n_e) is the ordinary(extraordinary) refractive index, we obtain for the maximum wedge excursion (45 mm) a delay $t_{1\,max}$=2.8 ps, corresponding to a frequency resolution $\Delta\lambda$=0.5nm at 650 nm [20]. After the TWINS interferometer, a 50% beam splitter divides the light into two arms. The reflected beam is focused on a photodiode (PD2, PDA36A, Thorlabs, Inc.), measuring the interferogram $\mathrm{I}_{\mathrm{ref}}\left(t_1\right)$, while the transmitted one is focused on the sample, contained in a 1-cm-thick cuvette. The light transmitted by the sample is focused on another photodetector (PD1, identical to PD2), measuring the interferogram $\mathrm{I}_{\mathrm{trans}}\left(t_1\right)$, while the fluorescence, collected at 90°, is collimated and focused on a spectrometer (Ocean Optics model USB2000) measuring the delay-dependent fluorescence spectrum $\mathrm{I}_{\mathrm{fluor}}\left(t_1,\omega_2\right)$, where ω_2 is the emission frequency. By computing a FT of the detected signals with respect to t_1, one simultaneously obtains the 2D EEM map $\tilde{\mathrm{I}}_{\mathrm{fluor}}\left(\omega_1,\omega_2\right)$ and the absorption spectrum A(ω_1). A pre-calibration measurement with a pure solvent in the cuvette holder is often required to properly retrieve A(ω_1), as described by Oriana *et al.* [20]. This is due to unmatched responsivities of PD1 and PD2 and different losses (mainly Fresnel reflections) along the two optical paths. This allows us to compute a frequency-dependent calibration curve c(ω_1), so that the absorption spectrum is computed as $\mathrm{A}\left(\omega_1\right)=-\log\left[c\left(\omega_1\right)\cdot\tilde{\mathrm{I}}_{\mathrm{trans}}\left(\omega_1\right)/\tilde{\mathrm{I}}_{\mathrm{ref}}\left(\omega_1\right)\right]$. Still, the main advantage of working with a reference arm is the removal of any intensity fluctuation of the light source. The setup is compact and has an unoptimized footprint of 40 cm×15 cm (if a LED is used as light source), which is significantly smaller than commercial EEM spectrometers.

3. Results

The time-domain spectrometer based on TWINS works in a partially rotating frame [16], as it introduces, for a given wedge insertion x (where x=0 is the position of the moving wedge corresponding to the zero path length difference), a frequency-dependent delay between the replicas $\mathrm{t}_1\left(\omega_1\right)=x\,\tan\alpha\left[\frac{1}{\mathrm{v}_{\mathrm{go}}\left(\omega_1\right)}-\frac{1}{\mathrm{v}_{\mathrm{ge}}\left(\omega_1\right)}\right]$ where $\mathrm{v}_{\mathrm{go}}\left(\mathrm{v}_{\mathrm{ge}}\right)$ is the group velocity of the ordinary(extraordinary) polarization. It is therefore important to perform a preliminary calibration of the setup. Figure 2(a) shows a zoom of the frequency-resolved linear autocorrelation $\mathrm{S}\left(x,\lambda_2\right)$ of the output of the supercontinuum fiber laser as a function of wedge insertion x and emission wavelength λ_2, as measured by placing the spectrometer directly in front of the TWINS, for a scan in the (-4mm; +4mm) range. By performing an FT with respect

to x, one obtains a function $\tilde{S}\left(f_x, \lambda_2\right)$, which, for each emission wavelength λ_2, peaks at a given value of the excitation spatial frequency f_x (see Fig. 2(b)). This allows us to uniquely associate an excitation wavelength λ_1 to any spatial frequency f_x. A vertical cut of Fig. 2(b) at λ_2=650 nm, after calibration, is shown as an inset of Fig. 2(b), demonstrating experimental excitation wavelength resolution $\Delta\lambda_1$=6 nm at FWHM for an 8-mm wedge excursion. If experimentally required, the resolution can be easily improved down to $\Delta\lambda_1 \approx 0.5$ nm by using the full scan range of our interferometer (45 mm).

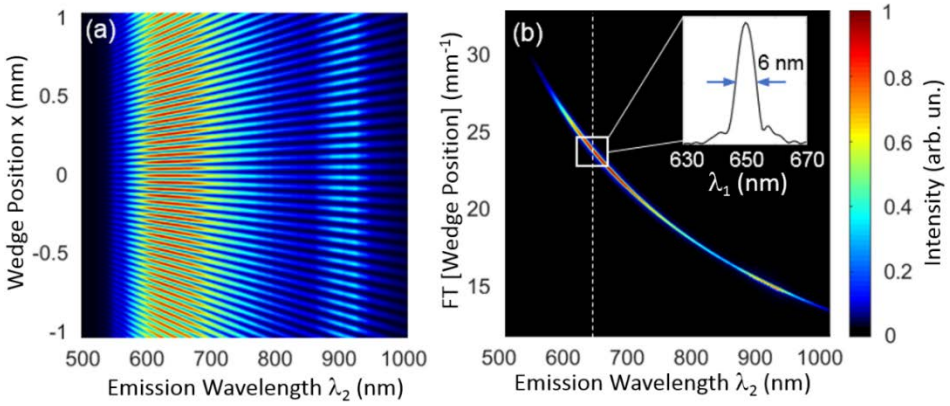

Fig. 2. (a) Zoom of the 2D linear autocorrelation, as a function of wedge position and emission wavelength, of the supercontinuum fiber laser. (b) 2D map as a function of spatial frequency (expressed in mm^{-1}) and emission wavelength, obtained by computing the FT of (a) as a function of wedge position, before calibration. Inset: calibrated spectrum as a function of excitation wavelength corresponding to the vertical cut in (b), showing a resolution of 6 nm.

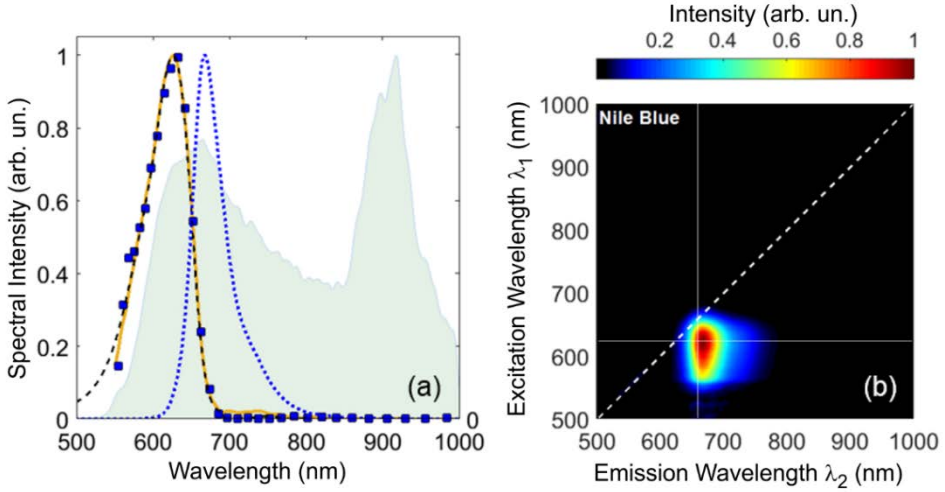

Fig. 3. (a) Normalized absorption spectrum of the dye Nile Blue in methanol solution, measured with the TWINS setup (solid yellow line) and with a commercial spectrophotometer (dashed black line), together with the fluorescence excitation spectrum (blue squares, resolution reduced for clarity), obtained as a vertical cut of the EEM map of Fig. 3(b) for the emission wavelength λ_2 = 660 nm. Fluorescence spectrum of Nile Blue in methanol solution, after excitation at 625 nm (dotted blue line). Spectrum of the supercontinuum fiber laser (light green area). (b) 2D EEM map of Nile Blue in methanol obtained with a total wedge excursion of 4mm, 800 spatial steps and 40 s acquisition time.

After the calibration of the excitation axis, we tested the ability of our setup to record absorption and emission spectra of a solvated dye sample, namely Nile Blue (LambdaChrome) solvated in HPLC-grade methanol. The maximum optical density was 0.5, as measured by a separate UV-Vis spectrophotometer (Jasco model V-550) and shown as a black dashed line in Fig. 3(a). It agrees perfectly with the absorption spectrum measured by TWINS. This demonstrates the accuracy of our wavelength calibration procedure. The $\tilde{I}_{fluor}(\lambda_1,\lambda_2)$ 2D EEM map shown in Fig. 3(b) was obtained by calibrating the $\tilde{I}_{fluor}(f_x,\lambda_2)$ with the calibration curve shown in Fig. 2(b). As a final step, we normalized each row of the EEM map at a given excitation wavelength by the light intensity of the light source at that wavelength (light green area in Fig. 3(a)). A horizontal cut through the 2D EEM map at λ_1=625 nm gives the fluorescence spectrum shown in Fig. 3(a) as a blue dotted line. A vertical cut of the EEM map for the emission wavelength λ_2=660 nm yields the fluorescence excitation spectrum, shown in Fig. 3(a) as filled blue squares. As expected, the fluorescence excitation spectrum closely matches the absorption spectrum, indicating that the same emissive state is reached regardless of excitation wavelength. We note that the total acquisition time for the well-resolved and high signal-to-noise ratio EEM map of Fig. 3(b) was only 40 s, which is faster than commercial frequency-domain spectrofluorometers using grating based monochromators.

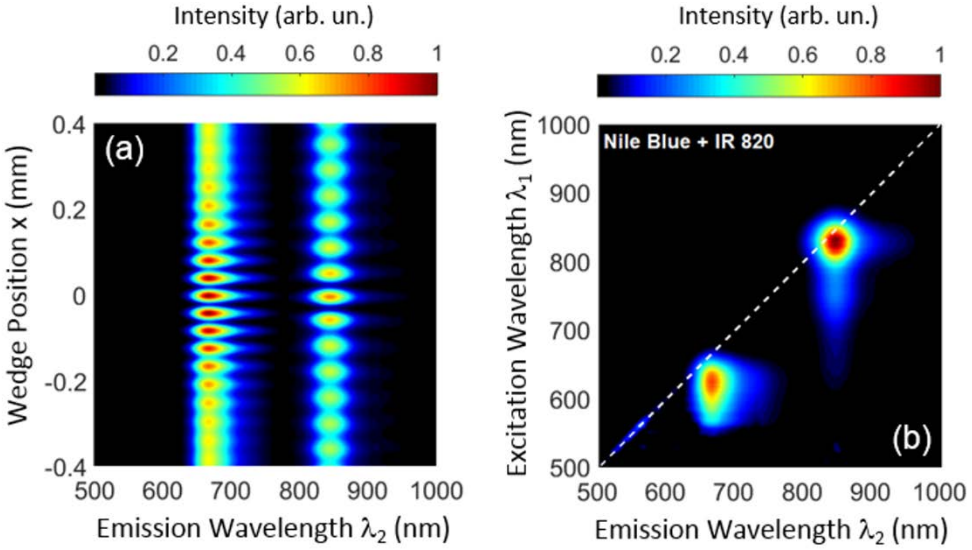

Fig. 4. (a) Zoom of the 2D EEM map of the mixture of the dyes Nile Blue (0.1 OD) and IR820 (0.45 OD) as a function of emission wavelength and wedge position Δx. The map was acquired in 13 minutes using 800 spatial steps and a 4 mm wedge excursion. (b) 2D EEM map as a function of excitation and emission wavelengths, obtained by performing the FT of the map in (a) with respect to x and applying the spectral calibration function.

2D EEM maps have the potential of clarifying spectrally congested regions where absorption and/or emission spectra of several species may overlap. In order to test this, we measured a mixture of Nile Blue and IR 820 (Aldrich) in methanol. Figure 4(a) shows a zoom of the 2D fluorescence map $I_{fluor}(x,\lambda_2)$ of the mixture as a function of wedge position and emission wavelength: one clearly observes the different periodicities of the interference patterns at λ_2=660 nm and λ_2 = 850 nm, corresponding to fluorescence emission from Nile Blue and IR 820, respectively. Figure 4(b) shows the corresponding 2D EEM map, obtained after the $x \rightarrow f_x$ FT and $f_x \rightarrow \lambda_1$ excitation-wavelength calibration. As we discussed for Fig. 2(b), also

this map is normalized with respect to the excitation light spectrum of Fig. 3(a). One clearly identifies the fluorescence peaks of the two dyes, red-shifted with respect to the absorption maxima, as well as a weak parasitic signal along the diagonal corresponding to unfiltered scattered excitation light (below 600 nm). The two signals on the EEM map are clearly separated, even though the respective absorption spectra partially overlap. Due to either the poor spectral overlap between the emission of Nile Blue and the absorption of IR 820, or to the large donor-acceptor distance, we observe no Förster resonant energy transfer between the species, which would give rise to a cross peak in the EEM map. One can notice that a portion of the fluorescence signals, in particular the IR 820 one, occurs at emission wavelengths shorter than the excitation ones. This is due to the limited spectral resolution on the excitation axis that is worse for longer wavelengths, causing a broadening of the features in the EEM maps.

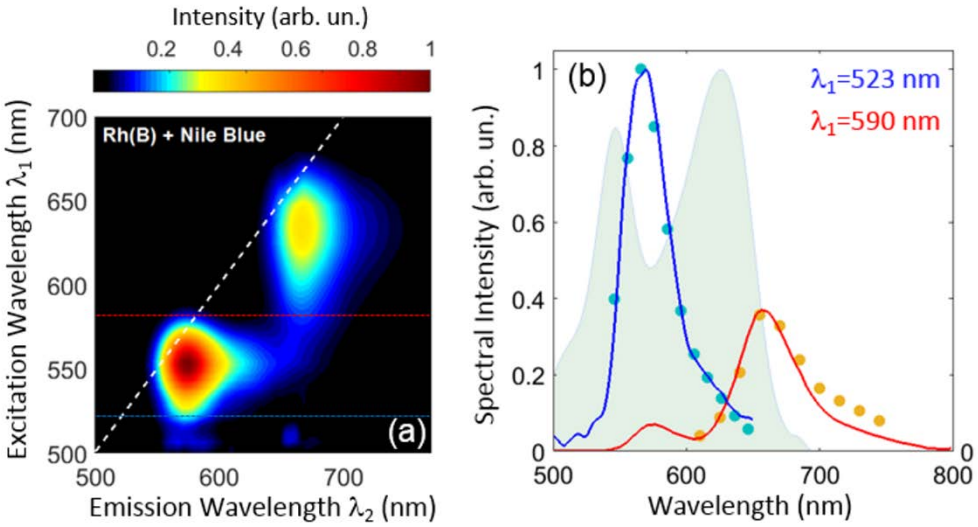

Fig. 5. (a) 2D EEM map for a mixture of Rhodamine B (0.35 OD) and Nile Blue (0.45 OD) dyes in Methanol measured with a white-light LED. The map is obtained with 1-mm wedge excursion, 200 spatial steps and total 16-minutes acquisition time. (b) Absorption spectrum of the dyes mixture (light green area) together with horizontal cuts of the EEM map (blue and red solid lines), corresponding to 523nm and 590nm excitation wavelength, in resonance mainly with Rhodamine B and Nile Blue, respectively. Blue and orange circles are fluorescence spectra taken from the literature [23].

All measurements described so far were performed using a spatially coherent supercontinuum fiber laser, which provides high brightness but significantly increases the instrument cost. In the following, we demonstrate that a low-cost spatially incoherent white-light LED can replace this source. In this case, particular care must be taken in properly collimating the beam along the optical path, to guarantee a good contrast of the interference fringes. This was achieved by placing a collimator in front of the light source. Figure 5(a) shows an example of EEM map measured with LED excitation. The sample is a mixture of two dyes: Nile Blue and Rhodamine B (LambdaChrome) dissolved in methanol. Blue and red solid lines in Fig. 5(b) show horizontal cuts of the map at λ_1=523 nm and λ_1=590 nm excitation wavelengths, which are predominantly resonant with Rhodamine B and Nile Blue, respectively. These are in excellent agreement with tabulated fluorescence spectra of the dyes [23], shown in Fig. 5(b) as circles. We note that EEM map obtained with LED illumination preserves the high quality of the data acquired with the laser. The main difference between coherent and incoherent excitation is the acquisition time for the EEM map, which is lowered by two orders of magnitude for coherent excitation under the same experimental conditions. Anyway, it is

faster than commercial setups based on scanning monochromators and incoherent illumination. We note that we could shorten the acquisition time even further in the future, irrespective of the desired spectral resolution, by proper undersampling. This technique is well known in the field of FT spectroscopy and consists in acquiring fluorescence spectra at wedge positions x separated by more than half of the interferogram period, i.e. below the Nyquist frequency [24]. This could significantly reduce the number of fluorescence spectra to be collected, especially when they have bandwidths considerably smaller than an octave.

4. Discussion, conclusions and outlook

In conclusion, we have presented a compact, fast and versatile spectrometer for the combined measurement of fluorescence, absorption, fluorescence excitation and 2D EEM spectra. Both incoherent and coherent light sources were successfully employed. The system is simple, compact, potentially low-cost and with fast acquisition times, offering advantages with respect to both commercial instruments based on monochromators and other proposed experimental schemes using time-domain FT approaches. The TWINS-based excitation stage increases the intensity of the fluorescence signal compared to a monochromator because the entire broadband spectrum of the light source illuminates the sample. In the case of spectrally scanned excitation, in fact, only a small portion of the excitation light spectrum is used at each step to generate the sample fluorescence. This causes a tenfold decrease of the spectrometer integration time to achieve the same fluorescence intensity.

Time-domain measurement of fluorescence excitation spectra using a FT approach has been proposed before in a number of studies. Hirschberg and coworkers performed interferometric measurements of fluorescence excitation spectra using a Michelson interferometer for generation of the excitation pulse pair and a photomultiplier for detection of the integrated fluorescence [11]. Peng *et al.* used a rapid-scanning FT spectrometer based on a Michelson interferometer for simultaneous measurement of fluorescence excitation spectra and excitation-wavelength dependent fluorescence lifetimes [25]. Piatkowski *et al.* used a time-domain approach, with phase-locked pulses generated by a Michelson interferometer with HeNe tracking beam, to record fluorescence excitation spectra of single molecules [13]. Finally, Anzai *et al.* recorded 2D EEM maps by the FT approach, using a tandem Fabry-Perot interferometer in excitation coupled with a diode array spectrometer on detection [12]. With respect to these configurations, our approach based on TWINS has clear advantages. Since it is a common-path interferometer, TWINS combines excellent delay accuracy with long-term stability without any active stabilization or delay tracking, greatly simplifying the setup and enabling to adapt the acquisition time to the signal level. With respect to the tandem Fabry-Perot interferometer, our setup has much higher light throughput, excitation frequency resolution and avoids parasitic spectral fringes.

For future developments, the CCD detector can be replaced by interferometric emission detection using TWINS and a high sensitivity single pixel detector, such as a photomultiplier or an avalanche photodiode, though at the cost of photon losses through the additional TWINS setup. While this will prolong data acquisition time, such a change in detection strategy will dramatically increase sensitivity while retaining the capability to record spectrally resolved signals. Such a spectrometer will be potentially of great interest to single molecule spectroscopy and imaging [13], as it would allow correlating spectral inhomogeneities in the electronic ground and excited states, by simultaneously measuring single-molecule fluorescence excitation (ground state) and fluorescence signals (excited state).

Funding

European Research Council: Consolidator Grant VIBRA (ERC-2014-CoG No. 648615), Advanced Grant STRATUS (ERC-2011-AdG No. 291198), Starting Grant SOLENALGAE (ERC-2015-StG No. 679814) and Proof of Concept Grant MISSION (ERC-2014-POC No.

665635). J. H. and E. T. acknowledge funding by the Austrian Science Fund (FWF): START project Y631−N27. G.C. and J.H acknowledge funding by Laserlab-Europe (EU-H2020 654148).